Original Article

JCBFM

Journal of Cerebral Blood Flow & Metabolism
2017, Vol. 37(7) 2509–2525

DOI: 10.1177/0271678X16669513
journals.sagepub.com/home/jcbfm
SAGE

Identification of two phosphorylation sites essential for annexin A1 in blood–brain barrier protection after experimental intracerebral hemorrhage in rats

Zhong Wang[1,*], Zhouqing Chen[1,*], Junjie Yang[2], Ziying Yang[2], Jia Yin[1], Gang Zuo[1], Xiaochun Duan[1], Haitao Shen[1], Haiying Li[1] and Gang Chen[1]

Abstract

Annexin A1 has been reported to exert a blood–brain barrier protection. This study was designed to examine the role of annexin A1 in intracerebral hemorrhage-induced blood–brain barrier dysfunction. A collagenase intracerebral hemorrhage model was performed in adult male Sprague Dawley rats. First, a possible relationship between annexin A1 and intracerebral hemorrhage pathology was confirmed by a loss of annexin A1 in the cerebrovascular endothelium and serum of intracerebral hemorrhage rats, and the rescue effects of i.v. administration of human recombinant annexin A1 in vivo and annexin A1 overexpression in vitro on the barrier function of brain microvascular endothelial cells exposed to intracerebral hemorrhage stimulus. Second, we found that intracerebral hemorrhage significantly increased the phosphorylation ratio of annexin A1 at the serine/threonine residues. Finally, based on site-specific mutagenesis, we identified two phosphorylation sites (a) annexin A1 phosphorylation at threonine 24 is required for its interaction with actin cytoskeleton, and (b) phosphorylation at serine27 is essential for annexin A1 secretion, both of which were essential for maintaining cytoskeleton integrity and paracellular permeability. In conclusion, annexin A1 prevents intracerebral hemorrhage-induced blood–brain barrier dysfunction in threonine 24 and serine27 phosphorylation-dependent manners. Annexin A1 phosphorylation may be a self-help strategy in brain microvascular endothelial cells after intracerebral hemorrhage; however, that was almost completely abolished by the intracerebral hemorrhage-induced loss of annexin A1.

Keywords

Intracerebral hemorrhage, secondary brain injury, blood–brain barrier, annexin A1, phosphorylation

Received 21 April 2016; Accepted 24 August 2016

Introduction

As a result of small vessel rupture within the brain parenchyma and the subsequent formation and expansion of the hematoma, spontaneous intracerebral hemorrhage (ICH) represents the most frequent, least treatable and deadliest stroke subtype.[1,2] In addition to the primary brain injury caused by the direct mechanical effects of the hemorrhage, ICH also leads to secondary brain injury (SBI), which has been shown to contribute to neurological deterioration after ICH.[3] Although increasing potential therapies targeting ICH-induced SBI have been proposed, the current clinical outcomes of ICH patients are still poor with only approximately 20% of ICH patients regaining functional independence at 6 months after ICH.[3,4]

As a peculiar system to cerebral vasculature, brain microvascular endothelial cell (BMVEC) and the dense and narrow tight junctions between adjacent endothelial

[1]Department of Neurosurgery, The First Affiliated Hospital of Soochow University, Suzhou, China
[2]Department of Cardiovascular Surgery, The First Affiliated Hospital of Soochow University, Suzhou, China
*These authors contributed equally to this work.

Corresponding authors:
Gang Chen, Department of Neurosurgery, The First Affiliated Hospital of Soochow University, 188 Shizi Street, Suzhou 215006, China.
Email: nju_neurosurgery@163.com
Haiying Li, Department of Neurosurgery, The first Affiliated Hosipital of Soochow University, 188 Shizi Street, Suzhou 215006, China.
Email: lhy1015@suda.edu.cn

cells form a selective permeability of the blood–brain barrier (BBB).[5] Over the past few decades, a lot of work has focused primarily on BBB integrity and indicated BBB breakdown or alteration as a complication in the pathogenesis of many CNS diseases, leading to failure of controlling transport across BBB and to the worsening of the pathologic conditions.[6,7] In addition, it is becoming increasingly clear that BBB permeability is focally increased in the hematoma, perihematoma, and ipsilateral hemisphere in acute ICH patients.[2,8] As a consequence of BBB disruption, leukocyte extravasation and perihematoma cerebral edema are main causes of SBI.[9,10] Despite seemingly diverse underlying mechanisms of BBB dysfunction, common intracellular pathways focus primarily on the regulation of the tight junction structural integrity.[11–13] A better understanding of tight junction regulation will allow the development of therapeutics to improve the BBB function in the presence and absence of pathology.[13]

For the small proportion of BMVECs in brain cells, double immunofluorescence staining with target protein antibody and vWF antibody-endothelial cell marker and Western blot analysis of the level of target protein in isolated brain capillaries have been the strategies for the study of expression of target protein in BMVECs in vivo.[14,15] In addition, the immortalized human brain endothelial cell line hCMEC/D3 has been a useful model of BBB in in vitro studies of the central nervous system (CNS).[16] In this study, we used all three methods to validate the protein level of annexin A1 (ANXA1) in BMVECs.

As a member of the annexin family of calcium-dependent phospholipid binding proteins, ANXA1 is identified as an essential endogenous regulator of BBB integrity in multiple sclerosis.[17] Briefly, intracellular ANXA1 and extracellular ANXA1 forming an autocrine/paracrine separately interact with actin cytoskeleton and formyl peptide receptor 2 (FPR2) to organize the inter-endothelial cell tight and adherens junctions and contribute significantly to BBB integrity and function.[17] However, until now no study has investigated the contribution of ANXA1 to BBB integrity after ICH. In addition, brefeldin A, a blocker of the classical endoplasmic reticulum (ER)-Golgi pathway for protein secretion, failed to inhibit ANXA1secretion in human immature lymphoblastic CCRF-CEM cell, suggesting that ANXA1 secretion is independent of the classical ER-Golgi pathway of exocytosis.[18] How ANXA1 is transported out of the cell is still poorly understood. Substantial evidence supports the view that the phosphorylation status is critical to ANXA1 localization, binding properties and functions.[19] Several kinases such as protein kinase C (PKC) have been shown to be responsible for the phosphorylation of selective residues in ANXA1.[19] In addition, PKC is activated under ICH condition.[20]

The aim of this study was to investigate the role of ANXA1 in ICH-induced SBI in rats, especially BBB dysfunction, and explore the effects of phosphorylation status on ANXA1 actions and even the specific phosphorylation sites.

Materials and methods

Experimental animals

All procedures were approved by the Institutional Animal Care Committee of the Soochow University and were performed in accordance with the guidelines of the National Institutes of Health on the care and use of animals. All animal research data have be written up in accordance with the ARRIVE (Animal Research: Reporting In Vivo Experiments) guidelines. Eight-week-old male Sprague Dawley (SD) rats weighing 250–300 g were provided by the Shanghai Experimental Animal Center of Chinese Academy of Sciences. The rats were housed at constant temperature (23°C) and relative humidity (40%) under a regular light/dark schedule. Food and water were available ad libitum. Sample sizes were determined by power analysis during the animal ethics dossier application.

Establishment of experimental ICH model in rats

A collagenase ICH model was performed as previously reported.[21] Briefly, SD rats were re-anesthetized (4% chloral hydrate, 10 ml/kg, i.p.) and fixed in a stereotaxic apparatus (ZH-Lanxing B type stereotaxic frame, Anhui Zhenghua Biological Equipment Co. Ltd., Anhui, China). Subsequently, 0.23 U collagenase VII infused with 1 μl physiological saline solution was injected slowly (5 min) unilaterally into the right striatum of the rats. Sham controls received an intracerebral injection of equal volume physiological saline solution. A schematic representation of the brain coronal sections is shown in Figure 1(a).

BMVEC culture and establishment of in vitro ICH model

The human cerebral microvascular endothelial cell line hCMEC/D3 was obtained from the Cell Bank of the Chinese Academy of Sciences (Shanghai, China). hCMEC/D3 cells were cultured as routine in 1640 medium (Hyclone, SH30809.01B) supplemented with 10% heat-inactivated fetal bovine serum and maintained at 37°C under humidified conditions and 5% CO_2. To mimic ICH, hCMEC/D3 cells were exposed to oxyhemoglobin (oxyHb, Ruibio, O7109) at the concentration of 10 μM.[22,23]

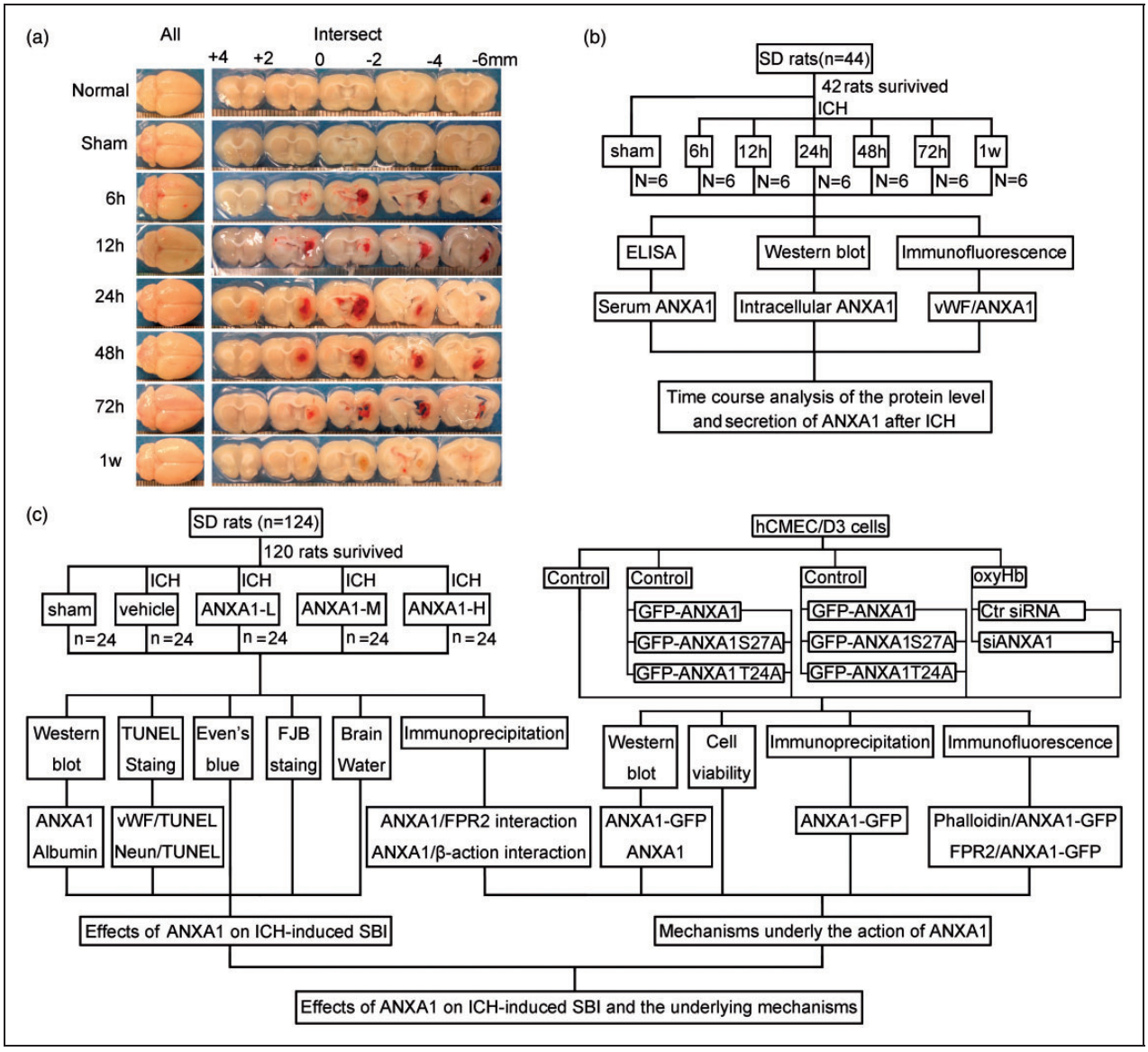

Figure 1. Intracerebral hemorrhage model and experimental design. (a) Brain coronal sections at the indicated time after infusion of collagenase. (b) Time course of the protein level and secretion of ANXA1 after ICH. (c) Effects of ANXA1 on ICH-induced SBI and the potential mechanisms. rhANXA1-L: 0.34 μg/kg body weight; rhANXA1-M: 0.67 μg/kg body weight; rhANXA1-H: 1.34 μg/kg body weight.

Experiment grouping

Part 1: Time course analysis of the protein level of ANXA1 after ICH. In in vivo experiment, 42 rats (44 rats were used, 42 rats were survived after the surgery) were randomly assigned to seven groups of six rats each, a sham group and six experimental groups arranged according to the following time points: 2 h, 12 h, 24 h, 48 h, 72 h, and 1 w after ICH. All the rats in the experiment were killed at the indicated time point after ICH. The brain cortex of six rats in each group was extracted and used for double immunofluorescence analysis and Western blot analysis, and blood was collected for serum ANXA1 concentration analysis (Figure 1(b)). An in vitro experiment was also performed to evaluate the effect of oxyHb treatment on the protein level of ANXA1 in hCMEC/D3 cells.

Part 2: Effects of ANXA1 on ICH-induced SBI and the underlying mechanisms. In in vivo experiments, 120 rats (124 rats were used, 120 rats were survived) were randomly divided into the following five groups (n = 24 per group): sham group, ICH + vehicle group, ICH + human recombinant ANXA1 (rhANXA1)-Low dosage group

(ANXA-L, 0.34 μg/kg body weight, i.v.), ICH + rhANXA1-Middle dosage group (ANXA-M, 0.67 μg/kg body weight, i.v.), and ICH + rhANXA1-High dosage group (ANXA-H, 1.34 μg/kg body weight, i.v.). The dosage of rhANXA1 was determined based on a previous study.[17] rhANXA1 was given at 3 h after collagenase injection, which was chosen based on the time needed for collagenase inducing hemorrhage in this ICH model. At 24 h after ICH, six rats per group were exsanguinated and used to isolate brain capillaries for Western blot analysis and immunoprecipitation analysis. Seventy-two hours after ICH, the brain cortexes of six rats per group were extracted for terminal deoxynucleotidyl transferase-mediated dUTP nick end labeling (TUNEL) staining, fluoro-jade B (FJB) staining, and six rats were used for evens blue staining to evaluate BBB disruption, while the remaining six rats per group were subjected to brain edema evaluation (Figure 1(c)).

Part 3: Mechanisms of ANXA1 actions. As shown in Figure 1(c), small RNA interference and site-directed mutagenesis studies have been performed in vitro to examine the mechanisms underlying the actions of ANXA1.

Antibodies

For details, please see the supplementary material.

Isolation of brain capillaries

Brain tissues were harvested from rats with indicated treatment. First, meninges and outer vessels were removed by rolling on dry cotton swabs. Then, cortices were sampled 1 mm away from the hematoma to avoid potential red blood cell contamination. Mechanical isolation of brain capillaries from cortices was performed as described previously.[14] Briefly, the tissues were ground by a Dounce homogenizer in 1 × HBSS 1 supplemented with 10 mM HEPES and 0.1% BSA. In addition, the homogenate was then mixed with 30% dextran (v/v, molecular weight 100,000–200,000) in 1 × HBSS containing 10 mM HEPES and 0.1% BSA. Subsequently, the resulting suspension was centrifuged at 3000 g for 25 min at 4°C. The dextran layer and the neural component were discarded, and the pellet containing the vascular component was resuspended in washing buffer (1 × HBSS 1 containing 10 mM HEPES and 0.1% BSA). Finally, to remove large vessels, the suspension was filtered through a 59 mm nylon mesh, which only allows the capillaries to pass.

Plasma membrane protein extraction

Plasma membrane protein extraction was performed using a membrane protein extraction kit (Biovision, K268-50), which can extract total cellular membrane proteins and purify plasma membrane proteins specifically. Briefly, the following two steps were performed: (a) extraction of total cellular membrane proteins; and (b) purification of plasma membrane proteins. All the reagent preparation and experimental operation were performed according to the manufacturer's instructions.

Western blot analysis

Protein samples (100 μg/lane) were loaded on a SDS-polyacrylamide gel, separated, and electrophoretically transferred to a polyvinylidene difluoride membrane (Millipore, IPVH00010), which was probed with primary antibodies and horseradish peroxidase-linked secondary antibodies, and subsequently revealed with an enhanced chemiluminesence detection kit. The relative quantity of proteins was analyzed by Image J program and normalized to that of loading controls. The quantitative analysis was performed by observers who were blind to experimental groups.

Ponceau S staining

As a sensitive method for protein determination, Ponceau S staining is considered as an alternative loading control in Western blots.[24,25] In this study, we performed Ponceau S staining to quantify the total protein of isolated microvessels. For details, please see the supplementary material.

Immunofluorescence analysis

For in vivo experiments, the brain samples were fixed in 4% paraformaldehyde, embedded in paraffin, cut into 4-μm sections, which was dewaxed immediately before immunofluorescence staining. For in vitro experiments, hCMEC/D3 cells were fixed in 4% paraformaldehyde. Then, sections and cells were stained with primary antibodies and appropriate secondary antibodies. Normal rabbit IgG was used as a negative control (data not shown). Finally, sections and cells were observed by a fluorescence microscope (OLYMPUS BX50/BX-FLA/DP70; Olympus Co., Japan) or a laser scanning confocal microscope (ZEISS LSM 880, Carl Zeiss AG, Germany). At least six random sections from each sample were examined, and representative results were shown. The relative fluorescence intensity was analyzed with the Image J program. The quantitative analysis was performed by an observer who was blind to the experimental group.

Enzyme-linked immunosorbent assay (ELISA)

The serum concentration of ANXA1 was determined by ELISA using the rat ANXA1 kit (USCN, SEE787Ra).

This assay was performed according to the manufacturer's instructions, and the data were expressed relative to a standard curve prepared for ANXA1.

TUNEL and FJB staining

TUNEL and FJB staining were performed as described previously.[26] For details, please see the supplementary material.

Cell viability

Cell viability was tested by Sulforhodamine B (SRB) assay. For details, please see the supplementary material.

FITC-dextran transwell assay

EC permeability was evaluated as described.[27] Briefly, hCMEC/D3 cells were plated on the insert of Transwell and cultured until confluent. FITC-dextran 150 (Invitrogen) was added to the top chamber. After 4–6 h, samples were removed from the basolateral (bottom) compartments and read in a fluorometer (Molecular Devices, FilterMax F5) at excitation 485 nm, emission 520 nm.

Construction of expression plasmids and site-directed mutagenesis

The coding region of human ANXA1 cDNA was sub-cloned into pEGFP-N2 expression vector to produce the pEGFPN2-ANXA1 construct. In addition, a human ANXA1 cDNA construct with a mutation in a possible key phosphorylation site (Ser27 or Thr24) was prepared. S27A mutant and T24A mutant (Ser27 and Thr24 of ANXA1 were mutated to alanine, respectively) were also sub-cloned into the pEGFP-N2 expression vector as the wild-type ANXA1 cDNA, which allowed us to measure their location by fluorescence assay. All of the constructs were confirmed by DNA sequencing.

siRNAs

To knock down ANXA1 expression, specific siRNAs against ANXA1 were obtained from GenScript. To improve the knockdown efficiency, the interference efficiency of three different siRNAs was tested, and the most efficient one was used in the following study. The ANXA1 siRNA sequences are shown in the supplementary material.

Transfection

hCMEC/D3 cells were plated onto dishes at a density 1×10^6/ml and grown for 24 h. When cell density reached 70–80% confluence, cells were transfected with indicated expression vectors using Lipofectamine® 3000 Transfection Reagent (Invitrogen, L3000-015) or siRNAs using Lipofectamine RNAi MAX (Invitrogen, 13778-075) according to the manufacturer's instructions. At 48 h after transfection, cells were exposed to oxyHb for 12 h. Then, the cells were harvested and analyzed by Western blot, immunofluorescence, and immunoprecipitation analysis. In addition, at 48 h after transfection cells were exposed to oxyHb for 24 h and then harvested for cell viability and FITC-Dextran Transwell assay.

Immunoprecipitation analysis

Immunoprecipitation analysis was performed as described previously.[26] For details, please see the supplementary material.

Rhodamine-phalloidin staining

Rhodamine phalloidin is one of the most commonly used fluorescent dyes of F-actin (Excitation/Emission: 540/565 nm). Rhodamine-phalloidin kit (Invitrogen, R415) was used, and all the reagent preparation and experimental operation were performed according to the manufacturer's instructions.

Statistical analysis

All data are presented as mean ± SEM. Graph pad prism 5 was used for all statistical analysis. One-way ANOVA for multiple comparisons and Student–Newman–Keulspost hoc test were used to determine the differences among all groups. $p < 0.05$ was considered to be significant difference.

Results

General observation

No significant changes in body weight, mean arterial blood pressure, temperature, or injected arterial blood gas data were detected in any of the experimental groups (data not shown). The mortality rate of rats in the sham group was 0% (0/30 rats), and it was 3.5% (6/168 rats) in the SAH group.

ICH decreased the protein levels of ANXA1 in BMVECs and serum

To detect the expression of ANXA1 in BMVECs during SBI after ICH, through Western blot analysis of protein samples from capillaries, we first tested the protein level of ANXA1 in the cerebral microvasculature. The results demonstrated that, compared with the

sham group, the protein level of ANXA1 in the microvascular endothelium was reduced significantly starting at 6 h after ICH, reached the lowest point at 24 h, and then rebounded gradually (Figure 2(a)). Consistent with the in vivo data, Western blot assay showed that the protein level of ANXA1 in cultured hCMEC/D3 cells was significantly decreased by oxyHb treatment at 6–18 h (Figure 2(b)). Double immunofluorescence with the endothelial marker protein vWF further verified the ICH-induced decrease in the protein level of ANXA1 in microvascular endothelium (Figure 2(c)). However, it is generally difficult to detect the sub-cellular localization of a protein by immunofluorescence staining of tissue sample sections. To clarify the effects of ICH stimulus on the protein level and sub-cellular localization of ANXA1 further, we performed immunofluorescence staining of ANXA1 on hCMEC/D3 cells treated with ICH stimulus in vitro. The results also showed an oxyHb-induced decrease in ANXA1 level and an accumulation of ANXA1 around the cell edge when compared with OxyHb group. In addition, ELISA analysis of the serum of rats were performed and showed that the serum content of ANXA1 significantly decreased 24 h after ICH and then rebounded to the corresponding level of sham group at 72 h (Figure 2(e)).

As shown above, there was a clear decrease in ANXA1 at 24 h after ICH. However, whether there is global down-regulation in endothelial cell protein expression induced by ICH or down-regulation specific to proteins such as ANXA1 is still not known. To answer this question, Ponceau S staining was performed, and the results showed that there was no significant different in the content of the total protein among each group, suggesting that the ICH-induced decrease in ANXA1 is specific (Supplementary Figure 1).

In vivo *rescue effects on BBB integrity of recombinant ANXA1*

As ANXA1 acts as an essential endogenous regulator of BBB integrity[17] and progressive breakdown of the BBB has been documented in ICH.[8] We examined the potential roles of ANXA1 on BBB integrity following ICH. The results showed that i.v. administration of rhANXA1 at 0.375–1.34 μg/kg body weight significantly reduced the degree of Evans blue dye extravasation into the brain, suggesting that rhANXA1 treatment effectively rescued the ICH-enhanced BBB leakage (Figure 3(a)). These findings were further confirmed by Western blot assay of brain content of albumin (Figure 3(b) and (c)). Notably, as compared with low-dosage rhANXA1 (0.375 μg/kg body), high-dosage rhANXA1 (1.34 μg/kg body) had a greater effect on improvement of BBB integrity of rats undergoing ICH (Figure 3(a)–(c)). Furthermore, it has been reported that ANXA1 contributes to BBB integrity by organizing the inter-endothelial cell tight and adherens junctions.[17] Here, we tested the effects of rhANXA1 treatment on the protein levels of two important inter-endothelial tight junction proteins, occludin and zona occludens 1 (ZO-1). The results showed that ICH induced a clear loss of occludin and ZO-1, while treatment with 1.34 μg/kg body weight rhANXA1 induced a significant up-regulation in the protein levels of occludin and ZO-1 (Figure 3(d) and (e)), thereby supporting a previous report that ANXA1 affects tight junction expression.[17] Subsequently, inter-endothelial tight junction redistribution could lead to BMVEC apoptosis,[5] which is an important mechanism causing the loss of cells, and as a result BBB dysfunction.[28] Finally, we performed TUNEL staining and found that only a few TUNEL-positive apoptotic cells were observed in the brain microvascular endothelium in the sham group, while the apoptotic index was found to be significantly higher in the ICH group. As compared with the ICH group, rhANXA1 at 0.67 μg/kg body and 1.34 μg/kg body exerted significant rescue effects on BMVEC apoptosis (Figure 3(f) and (g)). These results suggest that rhANXA1 treatment significantly improves BBB integrity and endothelial cell viability by protecting tight junction integrity.

However, these results could be interpreted in the following way: Dying and dead endothelial cells following ICH, as indicated by TUNEL labeling, are not going to be able to maintain junctions and they are going to down-regulate expression of most proteins including ANXA1, occludin, and so on. To test whether ICH-induced endothelial cell death leads to the loss of ANXA1 and occludin or ICH-induced ANXA1 and occludin loss leads to endothelial cell death, we tested the time cause assay of the protein levels of active-caspase3 and occludin following ICH (Supplementary Figure 2). The results showed that the protein level of active-caspase3 was significantly increased at 12 h, while the occludin protein level was significantly decreased at 9 h after oxyHb treatment in cultured BMVECs. Combined with the time cause assay of ANXA1 protein level shown in Figure 2, the loss of ANXA1 and tight junction protein occurred before BMVEC apoptosis. Previously, it has been reported that redistribution and degradation of tight junction proteins are the initial phase of BMVEC apoptosis.[5] Thus, we can conclude that ICH-induced ANXA1 and tight junction protein loss lead to endothelial cell death, which could be reversed by adding ANXA1 back into the system.

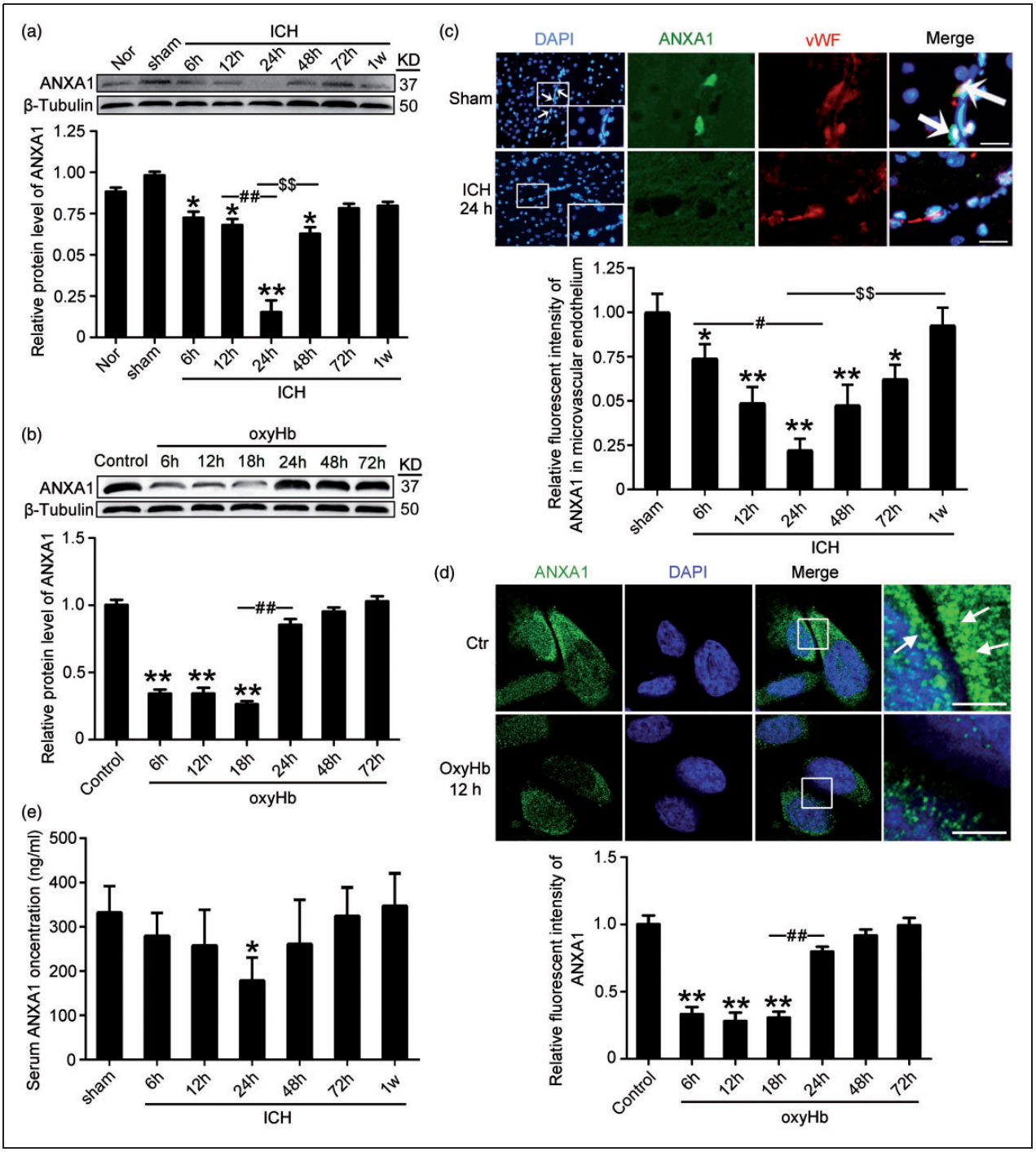

Figure 2. The protein levels of ANXA1 in microvascular endothelium and serum after ICH and oxyHb-treatment hCMEC/D3 cells. (a) Western blot analysis and quantification of the protein level of ANXA1 in brain capillaries. (b) Western blot analysis and quantification of the protein level of ANXA1 in hCMEC/D3 cells. (c) Double immunofluorescence analysis was performed with antibody for ANXA1 (green) and endothelial cell marker (vWF, red) in sections. Nuclei were fluorescently labeled with DAPI (blue). Representative images of the sham and ICH (24 h) groups are shown. Scale bar = 100 μm. The relative fluorescent intensity of ANXA1 in microvascular endothelium is shown below. (d) Immunofluorescence analysis was performed with antibody for ANXA1 (green) in cultured hCMEC/D3 cells under indicated treatment. Nuclei were fluorescently labeled with DAPI (blue). Representative images of control group and oxyHb (12 h) group are shown. Arrows indicate the accumulation of ANXA1 around the cell edge. Scale bar = 20 μm. In (a–d), mean values for sham or control group were normalized to 1.0. One-way ANOVA followed by Student–Newman–Keulspost hoc tests were used. Data are means ± SEM. (a) $^{*}p = 0.021$, 6 h group vs. sham group; $^{*}p = 0.018$, 12 h group vs. sham group; $^{*}p = 0.011$, 72 h group vs. sham group; $^{**}p < 0.01$ vs. sham group; $^{\#\#}p < 0.01$, $^{\$\$}p < 0.01$, n = 6. (b) $^{**}p < 0.01$ vs. sham group, $^{\#\#}p < 0.01$, n = 3. (c) $^{*}p = 0.032$, 6 h group vs. sham group; $^{*}p = 0.027$, 72 h group vs. sham group; $^{**}p < 0.01$ vs. sham group; $^{\#}p = 0.028$; $^{\$\$}p < 0.01$, n = 6. (d) $^{**}p < 0.01$ vs. control group; $^{\#\#}p < 0.01$, n = 3. (e) ELISA assay of the serum content of ANXA1. Data are means ± SEM. $^{*}p = 0.029$ vs. sham group, n = 6.

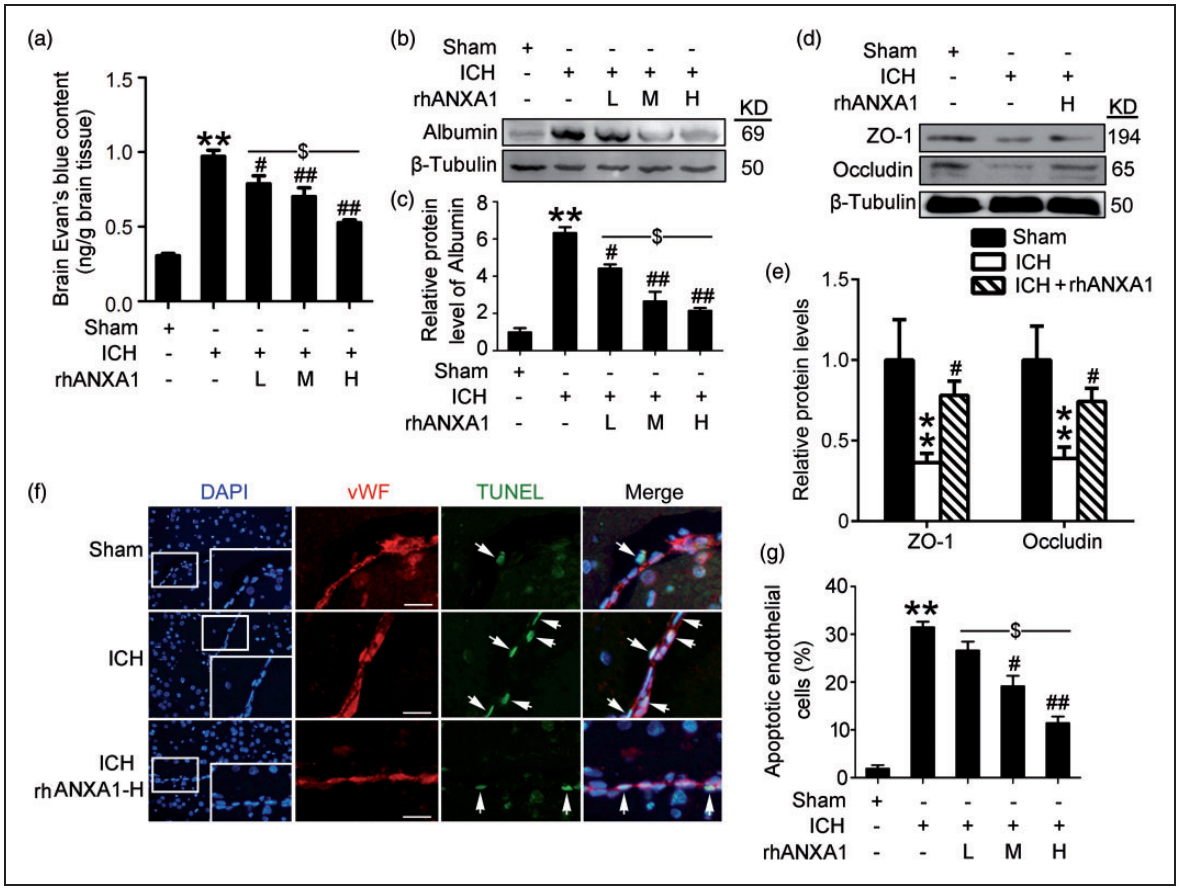

Figure 3. Effects of exogenous ANXA1 on BBB integrity in ICH rats. (a) The quantitative analysis of Evans blue content. Data are means ± SEM. $^{**}p < 0.01$ vs. sham group, $^{\#}p = 0.039$, $^{\#\#}p < 0.01$ vs. ICH group, $^{\$}p = 0.021$, n = 6. (b,c) Western blot assay of the albumin protein levels in brain. Protein levels were normalized to that of β-tubulin, and mean values for sham group were normalized to 1.0. In (c), data are means ± SEM. $^{**}p < 0.01$ vs. sham group, $^{\#}p = 0.024$, $^{\#\#}p < 0.01$ vs. ICH group, $^{\$}p = 0.019$, n = 6. (d,e) Western blot analysis and quantification of the protein level of zonula occludens-1 (ZO-1) and occludin. Protein levels were normalized to that of β-tubulin, and mean values for sham group were normalized to 1.0. Data are means ± SEM. $^{**}p < 0.01$ vs. sham group, $^{\#}p = 0.022$ in ZO-1, and $^{\#}p = 0.031$ in occludin vs. ICH group, n = 6. (f) Double immunofluorescence for vWF (red) and TUNEL (green) counterstained with DAPI (blue) was performed. Representative images of sham group, ICH (72 h) group and ICH (72 h) + rhANXA1-H group were shown. Arrows point to apoptotic endothelial cells, namely vWF/TUNEL-positive cells. Scale bar = 100 μm. Percentage of TUNEL-positive endothelial cells was shown (g). In (g), data are means ± SEM. $^{**}p < 0.01$ vs. sham group, $^{\#}p = 0.025$, $^{\#\#}p < 0.01$ vs. ICH group, $^{\$}p = 0.018$, n = 6. One-way ANOVA followed by Student–Newman–Keulspost hoc tests were used. rhANXA1-L: 0.34 μg/kg body weight; rhANXA1-M: 0.67 μg/kg body weight; rhANXA1-H: 1.34 μg/kg body weight.

In vivo *rescue effects on ICH-induced SBI of recombinant ANXA1*

To examine the effects of rhANXA1 on ICH-induced SBI, FJB and TUNEL staining were first performed to test neuronal degradation and neuronal death in the brain at 72 h after ICH. Compared with the sham group, FJB-positive cells were increased both in cortex and perihematoma brain in the ICH group, which was significantly attenuated by 0.67 μg/kg body and 1.34 μg/kg body rhANXA1 treatment (Figure 4(a)–(c)). Consistently, the neuronal death index showed the same trend (Figure 4(d) and (e)). Finally, brain water content was found to be significantly higher in brain samples of the ICH group than in rats subjected to the sham group. The mean brain water content was lower in rats with high-dosage rhANXA1 (1.34 μg/kg body) treatment than in the ICH control group (Figure 4(f)). These data highlight the rescue effects of rhANXA1 on ICH-induced SBI.

Recombinant ANXA1 rescued ICH-induced disruption in the interaction between ANXA1 and β-actin/FRP2

It has been reported that intracellular ANXA1 and extracellular ANXA1 could separately interact with the actin

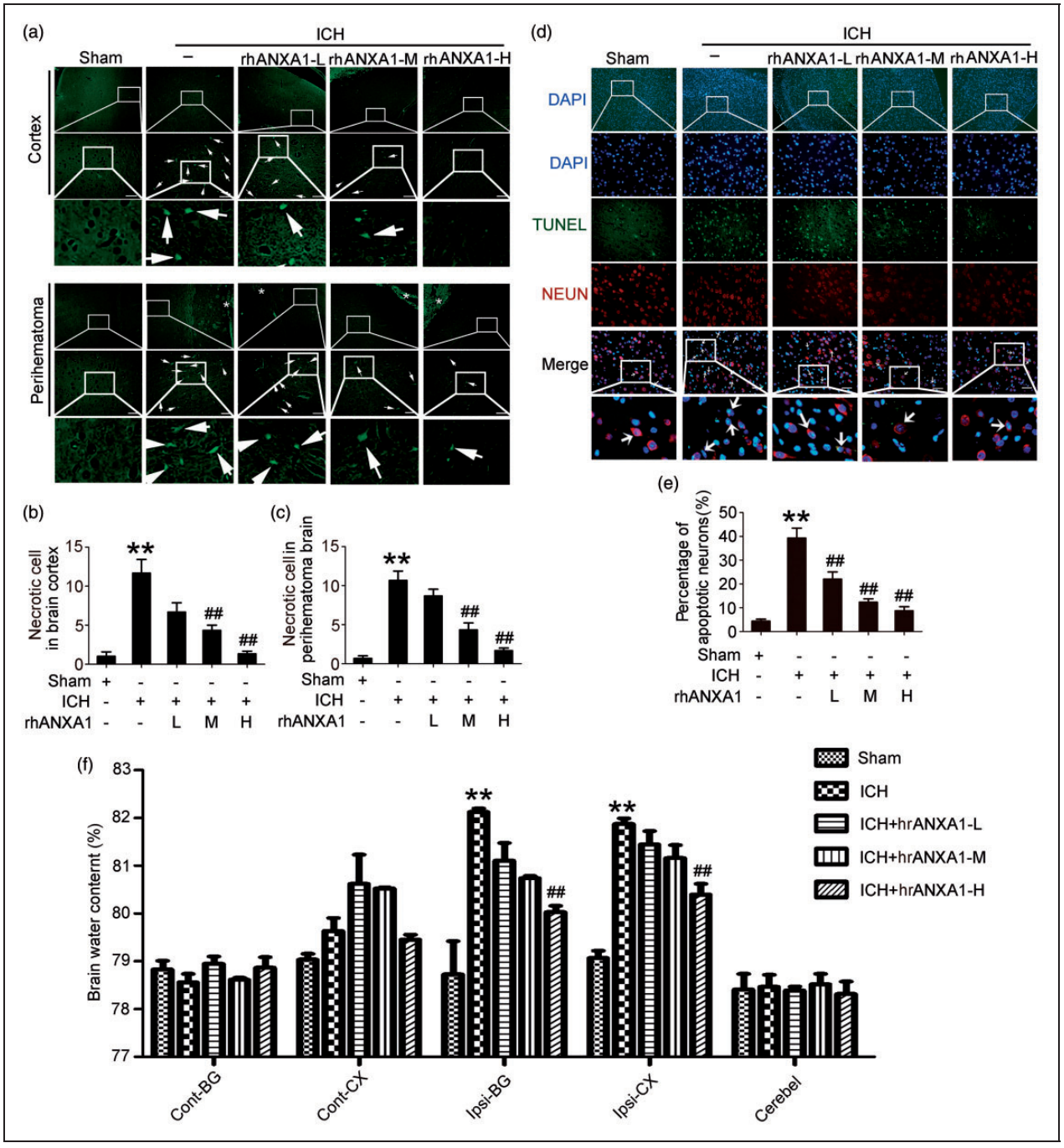

Figure 4. Effects of exogenous ANXA1 on neuronal degradation and death, and brain water content under ICH conditions. (a) Fluoro-Jade B (FJB) staining (green) shows neuronal degradation in cerebral cortex and perihematoma brain. Scale bar = 100 μm. Arrows point to FJB-positive cells. FJB-positive cells/mm^2 was quantified in brain cortex (b) and perihematoma brain (c), respectively. (d) Double immunofluorescence for NeuN (red) and TUNEL (green) counterstained with DAPI (blue) was performed. Arrows point to apoptotic neurons, namely NeuN/TUNEL-positive cells. Scale bar = 100 μm. Percentage of TUNEL-positive neurons was shown (e). (f) Bar graphs showing the effects of rhANXA1 on brain water content. Cont: contralateral; Ipsi: ipsilateral; CX: cortex; BG: basal ganglia; Cerebel; cerebellum. In (b,c,e,f), one-way ANOVA followed by Student–Newman–Keulspost hoc tests were used. Data are means ± SEM. $^{**}p < 0.01$ vs. sham group, $^{\#\#}p < 0.01$ vs. ICH group, n = 6. rhANXA1-L: 0.34 μg/kg body weight; rhANXA1-M: 0.67 μg/kg body weight; rhANXA1-H: 1.34 μg/kg body weight.

cytoskeleton and FPR2 to organize the inter-endothelial cell tight and adherens junctions.[17] To investigate the mechanism whereby rhANXA1 could rescue the permeability deficit seen in ICH rats further, we analyzed the interaction between ANXA1 and β-actin/FRP2 following ICH.[18] To examine the interaction between extracellular ANXA1 and FPR2 and avoid false positives induced by whole cell lysis lacking space positioning, plasma membrane protein extraction was performed. Immunoprecipitation experiments provided an interaction between ANXA1 and β-actin in whole cell lysis as well as between ANXA1 and FRP2 in plasma membrane protein extraction in sham group and identified a profound decrease in these interactions in ICH group, which was reversed by rhANXA1 treatment (Figure 5).

ICH induced phosphorylation of ANXA1, especially at ser27 and Thr24

Previous studies have indicated a critical role of ANXA1 phosphorylation in ANXA1 localization, binding properties and functions.[19] We then examined whether ICH could affect the phosphorylation status of ANXA1. Immunoprecipitated ANXA1 was subjected to Western blot analysis using antibodies against different phosphorylated amino acid residues. The results showed that the ICH group had a significantly increased phosphorylation ratio of ANXA1 at the serine and threonine residues (vs. sham group) but not the tyrosine residues (Figure 6(a)). PKC have been identified to be responsible for the phosphorylation of ANXA1[19] and PKC is activated following ICH[20]; therefore, we tested the effects of a PKC inhibitor (Santa Cruz, sc-3007) on the serine and threonine phosphorylation of ANXA1 in cultured BMVECs exposed to oxyHb (Supplementary Figure 3). The results showed that, compared with the OxyHb group, PKC inhibition significantly decreased the serine and threonine phosphorylation of ANXA1, suggesting that the increased ANXA1 phosphorylation following ICH is at least partially mediated by PKC. To elucidate the primary phosphorylation site of ANXA1

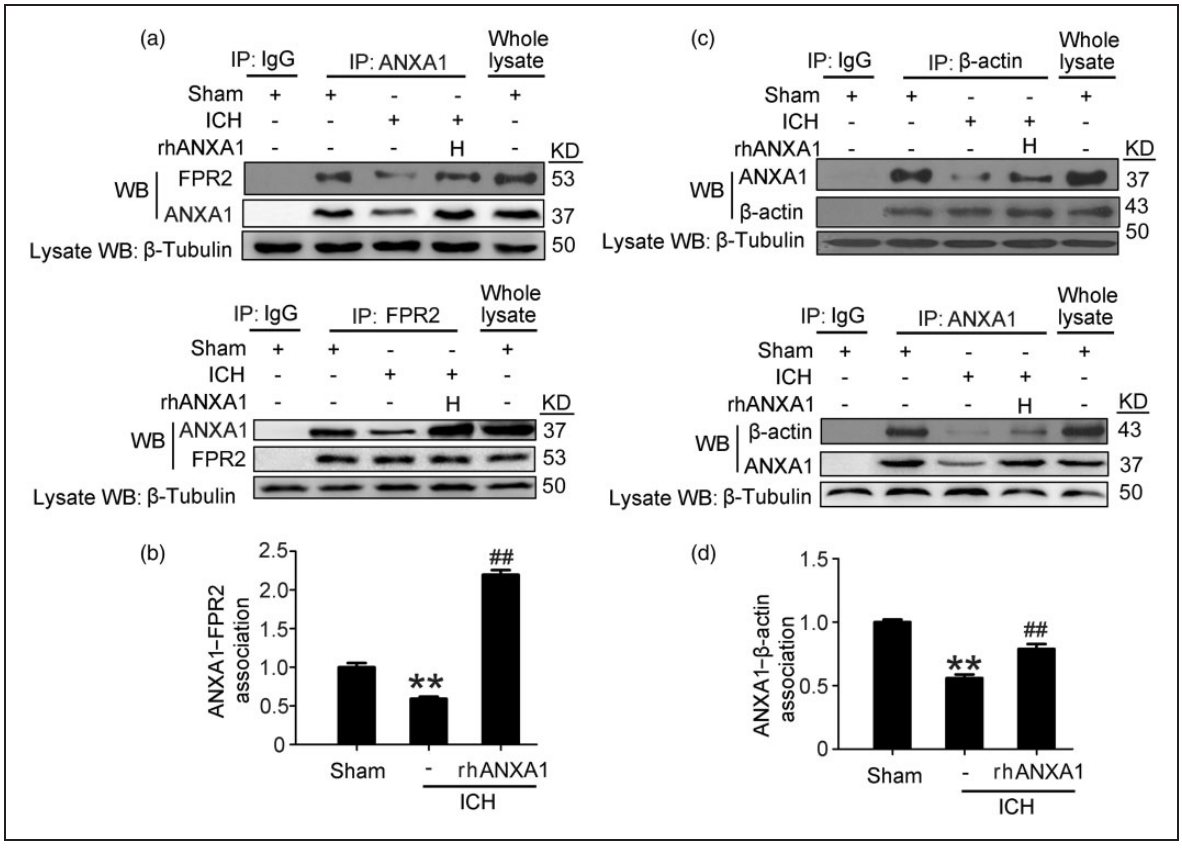

Figure 5. Effects of exogenous ANXA1 on ANXA1/FPR2 and ANXA1/β-actin interactions after ICH. (a,c) ANXA1/FPR2 interactions in plasma membrane protein extraction and ANXA1/β-actin interactions in whole lysis of brain capillaries were determined using immunoprecipitation (IP). (b,d) Quantitative histogram analysis was performed. One-way ANOVA followed by Student–Newman–Keulspost hoc tests were used. Data are expressed as mean ± SEM. $^{**}p < 0.01$ vs. sham group, $^{\#\#}p < 0.01$ vs. ICH group, n = 6. rhANXA1-H: 1.34 μg/kg body weight.

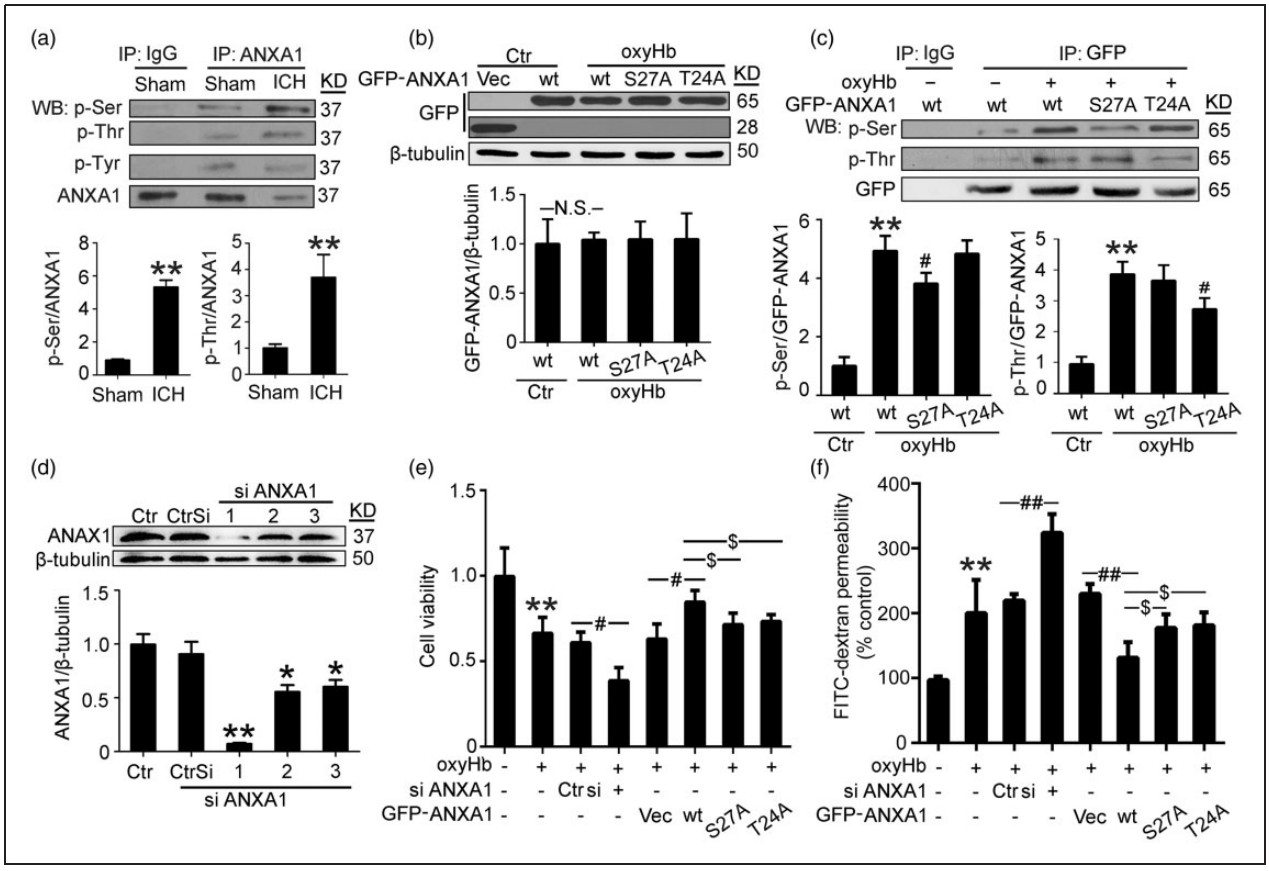

Figure 6. Effects of ICH on ANXA1 phosphorylation in brain capillaries and efficiency of ANXA1 siRNA and plasmid DNA transfections in cultured hCMEC/D3 cells. (a) Immunoprecipitation (IP) of cell lysates with ANXA1 antibody. Western blots of IP with indicated antibodies showed the phosphorylation of ANXA1 at the threonine residues, serine residues, and tyrosine residues. Quantification of the phosphorylation of ANXA1 at serine and threonine residues was shown. Data are expressed as mean ± SEM. $^{**}p < 0.01$ vs. sham group, n = 6. (b) hCMEC/D3 cells were transfected with expression vectors EGFP-N2, wide type EGFP-N2-ANXA1, EGFP-N2-ANXA1 (S27A), and EGFP-N2-ANXA1 (T24A). Cells were harvested 48 h after transfection. Equal amounts of indicated cell lysate proteins were immunoblotted using GFP antibody. Data are expressed as mean ± SEM. N.S.: no significant differences, n = 3. (c) Immunoprecipitation (IP) of cell lysates with GFP antibody. Western blots of IP with indicated antibodies showed the phosphorylation of wide type GFP-ANXA1 and GFP-ANXA1 mutants at the threonine residues and serine residues. Data are expressed as mean ± SEM. $^{**}p < 0.01$ vs. sham + wide type GFP-ANXA1, $^{\#}p = 0.032$ in p-Ser and $^{\#}p = 0.038$ in p-Thr vs. ICH + wide type GFP-ANXA1, n = 3. (d) ANXA1 silencing efficiency. $^{*}p = 0.038$ in siRNA-2 and $^{*}p = 0.048$ in siRNA-3, $^{**}p < 0.01$ vs. control siRNA, n = 3. (e) Cell viability of hCMEC/D3 cells with indicated treatment. Data are expressed as mean ± SEM. $^{**}p < 0.01$ vs. control, $^{\#}p = 0.032$ oxyHb + control siRNA vs. oxyHb + ANXA1 siRNA, $^{\#}p = 0.039$ oxyHb + vector vs. oxyHb + wide type GFP-ANXA1, $^{\$}p = 0.041$ oxyHb + wide type GFP-ANXA1 vs. oxyHb + GFP-ANXA1S27A, $^{\$}p = 0.043$ oxyHb + wide type GFP-ANXA1 vs. oxyHb + GFP-ANXA1T24A, n = 3. (f) FITC-dextran permeability of hCMEC/D3 cells with indicated treatment. Data are expressed as mean ± SEM. $^{**}p < 0.01$ vs. control group, $^{\#\#}p < 0.01$, $^{\$}p = 0.031$ oxyHb + wide type GFP-ANXA1 vs. oxyHb + GFP-ANXA1S27A, $^{\$}p = 0.029$ oxyHb + wide type GFP-ANXA1 vs. oxyHb + GFP-ANXA1T24A, n = 3. One-way ANOVA followed by Student–Newman–Keulspost hoc tests were used.

further, human ANXA1 cDNA constructs with mutation in possible key phosphorylation sites (S27 and T24) were prepared. These sites were selected based on previous studies that have implicated their importance in the actions of ANXA1.[19] First, both wild-type EGFP-ANXA1 and the mutant proteins were strongly expressed in transfected hCMEC/D3 cells, and oxyHb treatment did not affect the expression of exogenous ANXA1 (Figure 6(b)). Then, we examined the phosphorylation status of wide type and mutant proteins. The results showed that oxyHb induced the phosphorylation at the serine and threonine residues in wild-type EGFP-ANXA1, while both S27A and T24A mutants significantly abolished phosphorylation (Figure 6(c)), therefore supporting S27 and T24 as key sites for ICH-induced ANXA1 phosphorylation.

Rescue effects of ANXA1 on BMVEC permeability in a phosphorylation-dependent manner

We investigated whether a similar action of ANXA1 could be identified in the restoration of BBB function in vitro. The interference efficiency of three different siRNAs specific for ANXA1 was tested, and the most efficient one was used in the following study (Figure 6(d)). Compared with the control group, a significant decrease in BMVEC viability was observed in oxyHb group, which was exacerbated by ANXA1 knockdown and attenuated by wild-type EGFP-ANXA1 overexpression. However, rescue effects of ANXA1 on BMVEC viability was significantly abolished by serine27 or threonine 24 to alanine mutation (Figure 6(e)). In addition, by using a well-established method to examine the transendothelial permeability of a monolayer of BMVCEs, we showed that oxyHb-treated cells had significantly greater FITC-dextran permeability than control hCMEC/D3 cells, which was intensified by ANXA1 knockdown and suppressed by wild-type EGFP-ANXA1 overexpression. Mutations of serine27 or threonine 24 to alanine in ANXA1 significantly abolished its rescue effects on BMVEC permeability (Figure 6(f)).

Mutation of threonine 24 impairs the interaction of ANXA1 to β-actin

As shown in Figure 7(a), a clear biochemical interaction between wild-type EGFP-ANXA1 and β-actin in control group was identified by immunoprecipitation assay. OxyHb treatment further enhanced the interaction between wild-type EGFP-ANXA1 and β-actin, which was almost completely abolished by T24A mutation, suggesting a fundamental requirement of phosphorylation of ANXA1 at threonine 24 for the interaction of ANXA1 and β-actin. In addition, in the control group, the immunofluorescence assay revealed clear distribution of ANXA1 apparent alongside F-actin fibrils, as stained by rhodamine-phalloidin (Figure 7(b)), further indicating a previous reported role for ANXA1 in the formation/stabilization of the actin cytoskeleton.[17] Compared with the control group, fluorescence intensity of ANXA1 and F-actin fibrils in the oxyHb group was significantly decreased, especially the distribution of F-actin fibrils alongside the cell edge, which is critical for tight junctions formation. Compared with the EGFP group, wild-type EGFP-ANXA1 overexpression significantly rescued the oxyHb-induced disruption of F-actin fibrils, while threonine 24 to alanine mutation significantly abolished the rescue effects of wild-type ANXA1 (Figure 7(b)). Together, these results suggest that threonine 24 is essential for ANXA1 in organization actin cytoskeleton after ICH.

Mutation of serine27 impairs the secretion of ANXA1, which is critical for its interaction with FPR2

To investigate the potential roles of serine27 and threonine 24 in the secretion of ANXA1 further, we examined the impact of mutating these sites on the cultured supernatant content of ANXA1 using GFP-tagged constructs. Wild-type EGFP-ANXA1 was secreted by cultured hCMEC/D3 cells, but was unexpectedly significantly increased by oxyHb stimulation. However, unlike the EGFP-ANXA1-T24A, serine27 mutated to alanine almost completely abolished the secretion of ANXA1 after oxyHb stimulation (Figure 7(c)). In addition, consistent with the trend of the cultured supernatant content of ANXA1, the interaction between wild-type EGFP-ANXA1 and FPR2 was enhanced by oxyHb treatment and almost completely abolished by S27A mutation (Figure 7(d)). Interestingly, the phosphorylation level of immunoprecipitated EGFP-ANXA1 protein was too low to detect, suggesting that ANXA1 may undergo dephosphorylation outside the cells after secretion and before the interaction with FPR2. Together, these results suggest that serine27 is essential for ANXA1 secretion, which is critical for the interaction between ANXA1 and FPR2.

Discussion

As previously reported[17] and shown here, the essential role of ANXA1 in maintaining the integrity of the BBB, and the loss of ANXA1 in cerebral capillaries in multiple sclerosis and ICH, suggest that therapies targeting ANXA1 hold significant promise for the treatment and prevention of pathologic processes characterized by compromised BBB function. Using site-directed mutagenesis of potential key phosphorylation residues to alanine in ANXA1, we have shown for the first time that the molecular mechanism by which ANXA1 interacts with β-actin and secretes from BMVECs requires its phosphorylation on threonine 24 and serine27, respectively. Consistently, it has been reported that lipopolysaccharide induced phosphorylation of ANXA1 at serine27 is a fundamental requirement for cellular exportation of ANXA1 in pituitary folliculostellate cells.[29] Thus, the complete understanding of ANXA1 physiological changes due to different phosphorylation states could lead to new models and therapeutic approaches in treatment of cerebrovascular disease.

This study focused on the ANXA1 phosphorylation status and its possible role in regulation of the ANXA1 functions following ICH. As a commonly used tag for protein studies, GFP was used to fuse with ANXA1 to distinguish the endogenous and exogenous ANXA1. As phosphorylation is the critical index for this study, we

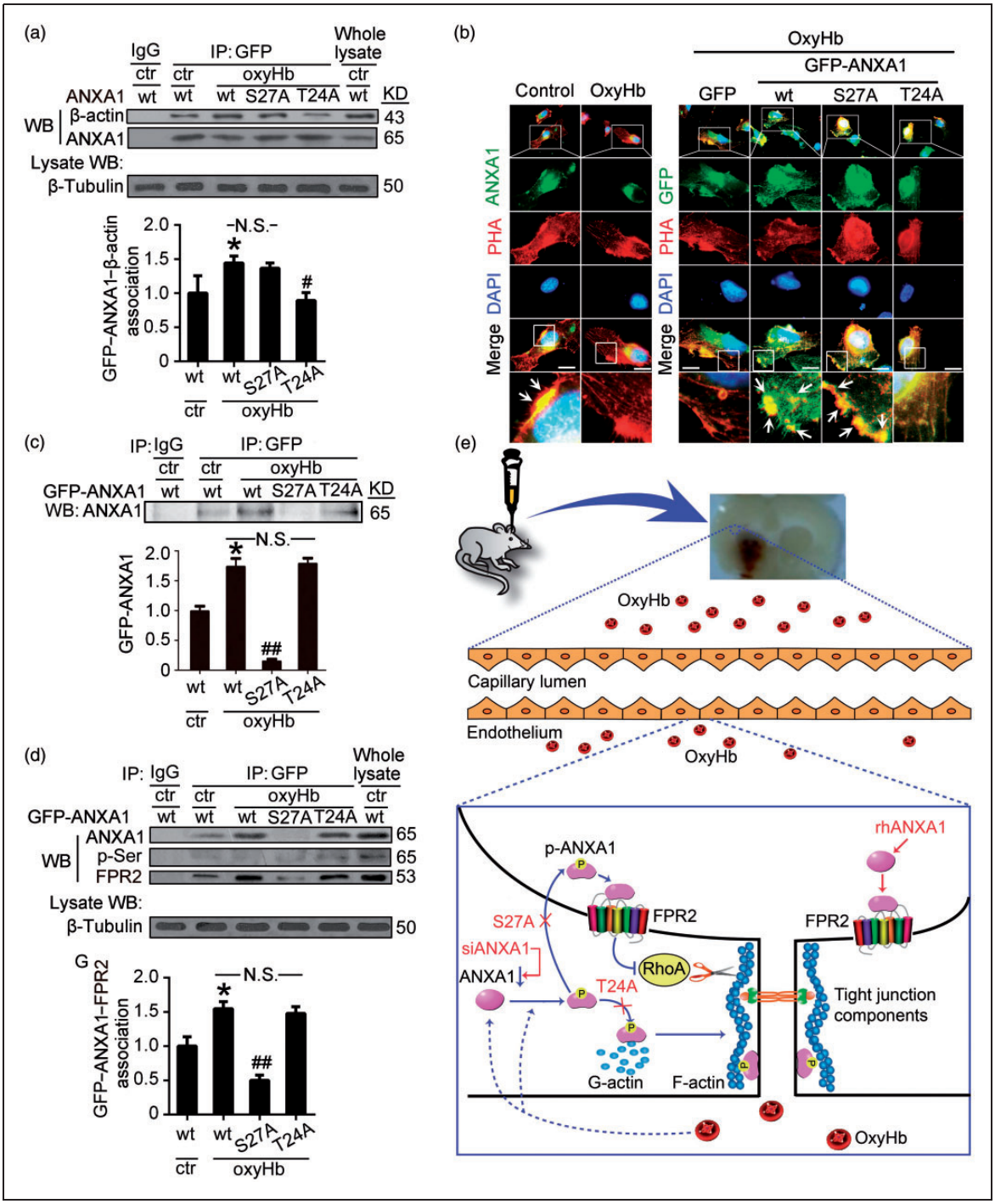

Figure 7. Effects of mutation of serine27 or threonine 24 to alanine on ANXA1 actions. (a) Immunoprecipitation (IP) of cell lysates with GFP antibody. Western blots of IP with β-actin antibody showed the interactions between wild-type GFP-ANXA1 or GFP-ANXA1 mutants and β-actin. (b) Rhodamine-phalloidin staining of F-actin in hCMEC/D3 cells with indicated treatments. Arrows indicated the overlap of ANXA1 and F-actin around the cell edge. PHA: phalloidin. Scan bar = 20 μm. (c) Immunoprecipitation (IP) of cultured supernatant with GFP antibody. Western blots of IP with ANXA1 antibody showed the cultured supernatant content of wild-type GFP-ANXA1 and GFP-ANXA1 mutants. (d) Immunoprecipitation (IP) of plasma membrane protein of hCMEC/D3 cells with indicated treatments. Western blots of IP with FPR2 antibody showed the interactions between wild-type GFP-ANXA1 or GFP-ANXA1 mutants and FPR2. In (a,c,d), one-way ANOVA followed by Student–Newman–Keulspost hoc tests were used. Data are expressed as mean ± SEM. In (a), $^{*}p = 0.043$ vs. control + wide type GFP-ANXA1 group, $^{\#}p = 0.039$ vs. oxyHb + wide type GFP-ANXA1 group, N.S.: no significant differences, n = 3. In (c), $^{*}p = 0.018$ vs. control + wide type GFP-ANXA1 group, $^{\#\#}p < 0.01$ vs. oxyHb + wide type GFP-ANXA1 group, N.S.: no significant differences, n = 3. In (d), $^{*}p = 0.023$ vs. control + wide type GFP-ANXA1 group, $^{\#\#}p < 0.01$ vs. oxyHb + wide type GFP-ANXA1 group, N.S.: no significant differences, n = 3. (e) Schematic representations of potential mechanisms of ANXA1 phosphorylation in maintaining BBB integrity under ICH condition. Blue colored arrows indicate the ICH-induced ANXA1 actions, and red colored arrows indicate the effects of rhANXA1, siANXA1 and mutation of serine27 or threonine 24 to alanine on ANXA1 actions.

confirmed the phosphorylation of GFP-ANXA1 after tagging. As shown in Figure 6(a) and (c), under ICH condition, ANXA1 phosphorylation and GFP-ANXA1 phosphorylation shared the same trend, suggesting that fusion with GFP did not affect ICH-induced ANXA1 phosphorylation. Besides phosphorylation, substantial evidence also supports essential roles of other post-translational modifications, including SUMOylation and ubiquitination in the actions of ANXA1.[30] In addition, there is cross talk among these post-translational modifications. For example, phosphorylation of tyrosine 21 is crucial for epidermal growth factor-induced ANXA1 SUMOylation.[31] In addition, the authors have also shown the relevance of tyrosine 21 phosphorylation for the ANXA1 stability.[31] Whether other post-translational modifications are involved in ANXA1 protein level regulation under ICH condition needs further investigation.

It is well known that one protein level can be regulated by both the expression and the degradation of the protein. As shown in Figure 2(a) and (e), ICH decreased the protein levels of ANXA1 both in capillaries and serum, while oxyHb treatment did not affect the protein level of EGFP-ANXA1 (Figure 6(b)), suggesting that ICH condition mimicked by oxyHb treatment attenuated ANXA1 expression at transcriptional level.

Most secretory proteins contain amino internal or terminal signal peptides that direct their sorting to ER and are transported to the plasma membrane or extracellular space via a process known as conventional secretion pathway or ER-Golgi secretory pathway.[32] However, the ER-Golgi system is not suitable for some leaderless secreted proteins.[32] In mammalian systems, current studies have suggested an unexpected role of autophagy in protein trafficking and secretion. In other words, autophagy-based unconventional secretion, also termed ''autosecretion,'' is an unconventional secretion pathway enabling leaderless cytosolic proteins to exit the cell without entering ER-Golgi secretory pathway. Annexins do not contain signal peptides, yet some annexins (ANXA1, ANXA2, and ANXA5) appear to be secreted in a physiologically regulated fashion. Among annexin family members, ANXA2, ANXA5, and ANXA7 have been shown to participate in autophagy regulation.[33–35] However, the function of ANXA1 in autophagy and whether ANXA1 is secreted via autosecretion is not clear. In addition, as shown in Figure 5(a), rhANXA1 treatment increases ANXA1 protein levels in microvessels, which can be interpreted in the following two ways: recombinant protein is getting into brain microvessels or there may be a negative regulation mechanism in ANXA1 secretion. Considering the negative regulation mechanism, rhANXA1 treatment induces a high extracellular ANXA1 concentration and subsequently inhibits the extracellular secretion of the endogenous ANXA1 finally resulting in an increased ANXA1 protein level in microvessels. To distinguish the mechanism further, we used overexpression of GFP-ANXA1, which could be distinguished from endogenous ANXA1 and rhANXA1 and tested the effects of rhANXA1 treatment on the extracellular secretion of GFP-ANXA1 in oxyHb-treated BMVECs (Supplementary Figure 4). The results showed that rhANXA1 treatment significantly decreased the extracellular concentration of GFP-ANXA1. Based on these results, we concluded that the negative regulation of ANXA1 secretion induced by rhANXA1 treatment might exist and lead to the increased ANXA1 protein levels in microvessels. However, the exact mechanism underlying the negative regulation needs further study.

In addition, as shown in Figure 3, rat treatment with exogenous ANXA1 showed positive effects on ICH-induced BBB dysfunction. However, in vivo rescue effects on ICH or induced SBI by rhANXA1 are not complete (Figure 4). An increasing number of reports have suggested that with the continuous improvement of surgical techniques and medical devices the mortality and morbidity of ICH in clinical are still surprisingly high.[36–38] In addition, the failure of therapies solely targeting one cell type in isolation has been identified as ''translational roadblock'' in stroke research.[39] The concept of a neurovascular unit was first described by Zvi Cohen in 1996 as an elaborate web of microvessels in the brain, and has attracted a lot of attention in stroke research.[40,41] As the anatomical substrate of the BBB, BMVECs together with neurons, astrocytes, pericytes, microglia/macrophages, and the extracellular matrix, constitute a ''neurovascular unit,'' which is essential for the function and health of the CNS.[42] Thus, protecting the cells and matrices that support BMVECs might be as important as protecting the BMVECs themselves. A key to overcoming the incomplete rescue of exogenous ANXA1 on ICH or induced SBI may be the new appreciation that aims the neurovascular unit as an integral part in the pathological process of ICH-induced SBI.

In this study, we only focused on the role of ANXA1 on BBB permeability. As shown in Figure 4, rhANXA1 treatment seems to ameliorate ICH-induced neuronal cell death, which could be interpreted by the rescue effects of rhANXA1 treatment on BBB integrity. However, there may be direct effects of rhANXA1 treatment on neuronal cell death. For example, TRPM7 channel-kinase has been shown to play key roles in regulating intracellular magnesium homeostasis and in anoxic neuronal death.[43] In addition, TRPM7 kinase could induce ANXA1 phosphorylation at a conserved serine residue (serine5). Serine5, threonine 24,

and serine27 are all located at the N-terminal of ANXA1 region, which plays a crucial role in the interaction of ANXA1 with membranes and other proteins. Moreover, as shown in Figure 6, site-directed mutagenesis of serine27 and threonine 24 to alanine inhibited oxyHb-induced wide type ANXA1 phosphorylation at approximately 50%, which is consistent with substantial evidence that different kinases have been identified to mediate ANXA1 phosphorylation on several residues.[19] Therefore, besides tight junction regulation, ANXA1 might have other targets and functions for explaining its protective effect for neuronal cell death, such as TRPM7 kinase-induced ANXA1 phosphorylation.

Besides an essential endogenous regulator of BBB integrity,[17] ANXA1 is also a well-known anti-inflammatory mediator.[44] As the pivotal role of inflammatory responses in ICH-induced SBI,[45] the anti-inflammatory role of ANXA1 may be vital to the protective effect of rhANXA1 on SBI in the ICH model. It has been reported that ANXA1 is present in different molecular forms in rat cerebral cortex.[46] The ANXA1 form with an apparent relative molecular mass of 37 kDa has phospholipase A2 inhibitory activity and exerts anti-inflammatory effects.[44] As shown in this study, we detected ANXA1 at approximately 37 kDa. ANXA1 was shown to inhibit the activation of NF-kappaB by binding to the p65 subunit, which regulates multiple inflammation responses following ICH.[47] A novel anti-inflammatory mechanism of high-density lipoprotein through up-regulating ANXA1 in vascular endothelial cells has also been reported.[48] All these reports and results suggest that the anti-inflammatory effects of ANXA1 may participate in the protective effect of rhANXA1 on ICH-induced SBI.

In conclusion, the present study demonstrated that following ICH, the release of hematoma components such as oxyHb induced a decrease in the protein level of ANXA1 and an increased ratio in the phosphorylation of ANXA1. ANXA1 phosphorylation at threonine 24 is required for its interaction with β-actin, while ANXA1 secretion is dependent on phosphorylation at serine27. As reported previously reported, intracellular ANXA1 binds to G-actin, promoting F-actin formation, while extracellular ANXA1 acting via FPR2 inhibits RhoA activity, contributing to the stability of cytoskeleton and enhancing tight junction formation, hence promoting BBB integrity.[17] Thus, ANXA1 phosphorylation may be a self-help strategy in BMVECs after ICH; however, that was almost completely abolished by the ICH-induced loss of ANXA1. Intriguingly, the hypothesis highlights the potential utility of exogenous ANXA1 in maintaining BBB integrity after ICH, which was identified in an experimental rat ICH model for the first time in this study (Figure 7(e)).

Funding

The author(s) disclosed receipt of the following financial support for the research, authorship, and/or publication of this article: Suzhou Key Medical Center (Szzx201501), National Natural Science Foundation of China (No. 81571115, 81422013, and 81471196), Scientific Department of Jiangsu Province (No. BL2014045), Education Department of Jiangsu Province (No. 16KJB320008), Suzhou Government (No. LCZX201301, SZS201413, SYS201332, and SYS201608), and a project funded by the Priority Academic Program Development of Jiangsu Higher Education Institutions.

Authors' contributions

Gang Chen and Haiying Li conceived and designed the study. Zhong Wang and Zhouqing Chen performed the experiments and wrote the paper. Junjie Yang and Ziying Yang assisted the use of laser scanning confocal microscope. Jia Yin and Gang Zuo helped conduct the literature review. Xiaochun Duan and Haitao Shen reviewed and edited the manuscript. All authors read and approved the manuscript.

Declaration of conflicting interests

The author(s) declared no potential conflicts of interest with respect to the research, authorship, and/or publication of this article.

Supplementary material

Supplementary material for this paper can be found at http://jcbfm.sagepub.com/content/by/supplemental-data

References

1. Ma Q, Huang B, Khatibi N, et al. PDGFR-alpha inhibition preserves blood-brain barrier after intracerebral hemorrhage. *Ann Neurol* 2011; 70: 920–931.
2. Selim M and Sheth KN. Perihematoma edema: a potential translational target in intracerebral hemorrhage? *Transl Stroke Res* 2015; 6: 104–106.
3. Urday S, Kimberly WT, Beslow LA, et al. Targeting secondary injury in intracerebral haemorrhage–perihaematomal oedema. *Nat Rev Neurol* 2015; 11: 111–122.
4. Xi G, Strahle J, Hua Y, et al. Progress in translational research on intracerebral hemorrhage: is there an end in sight? *Progr Neurobiol* 2014; 115: 45–63.
5. Li H, Gao A, Feng D, et al. Evaluation of the protective potential of brain microvascular endothelial cell autophagy on blood-brain barrier integrity during experimental cerebral ischemia-reperfusion injury. *Transl Stroke Res* 2014; 5: 618–626.
6. Liu WY, Wang ZB, Wang Y, et al. Increasing the permeability of the blood-brain barrier in three different models in vivo. *CNS Neurosci Therap* 2015; 21: 568–574.
7. Yang L, Tang J, Chen Q, et al. Hyperbaric oxygen preconditioning attenuates neuroinflammation after intracerebral hemorrhage in rats by regulating microglia characteristics. *Brain Res* 2015; 1627: 21–30.

8. McCourt R, Gould B, Kate M, et al. Blood-brain barrier compromise does not predict perihematoma edema growth in intracerebral hemorrhage. *Stroke* 2015; 46: 954–960.
9. Keep RF, Hua Y and Xi G. Intracerebral haemorrhage: mechanisms of injury and therapeutic targets. *Lancet Neurol* 2012; 11: 720–731.
10. Keep RF, Zhou N, Xiang J, et al. Vascular disruption and blood-brain barrier dysfunction in intracerebral hemorrhage. *Fluids Barriers CNS* 2014; 11: 18.
11. Nico B and Ribatti D. Morphofunctional aspects of the blood-brain barrier. *Curr Drug Metab* 2012; 13: 50–60.
12. Huber JD, Egleton RD and Davis TP. Molecular physiology and pathophysiology of tight junctions in the blood-brain barrier. *Trends Neurosci* 2001; 24: 719–725.
13. Persidsky Y, Ramirez SH, Haorah J, et al. Blood-brain barrier: structural components and function under physiologic and pathologic conditions. *J Neuroimmune Pharmacol* 2006; 1: 223–236.
14. Coisne C, Dehouck L, Faveeuw C, et al. Mouse syngenic in vitro blood-brain barrier model: a new tool to examine inflammatory events in cerebral endothelium. *Lab Invest* 2005; 85: 734–746.
15. Li H, Wang Y, Feng D, et al. Alterations in the time course of expression of the Nox family in the brain in a rat experimental cerebral ischemia and reperfusion model: effects of melatonin. *J Pineal Res* 2014; 57: 110–119.
16. Vu K, Weksler B, Romero I, et al. Immortalized human brain endothelial cell line HCMEC/D3 as a model of the blood-brain barrier facilitates in vitro studies of central nervous system infection by Cryptococcus neoformans. *Eukar Cell* 2009; 8: 1803–1807.
17. Cristante E, McArthur S, Mauro C, et al. Identification of an essential endogenous regulator of blood-brain barrier integrity, and its pathological and therapeutic implications. *Proc Natl Acad Sci USA* 2013; 110: 832–841.
18. Castro-Caldas M, Duarte CB, Carvalho AP, et al. Dexamethasone induces the secretion of annexin I in immature lymphoblastic cells by a calcium-dependent mechanism. *Mol Cell Biochem* 2002; 237: 31–38.
19. D'Acunto CW, Gbelcova H, Festa M, et al. The complex understanding of Annexin A1 phosphorylation. *Cell Signall* 2014; 26: 173–178.
20. Cui GY, Gao XM, Qi SH, et al. The action of thrombin in intracerebral hemorrhage induced brain damage is mediated via PKCalpha/PKCdelta signaling. *Brain Res* 2011; 1398: 86–93.
21. Rolland WB, Lekic T, Krafft PR, et al. Fingolimod reduces cerebral lymphocyte infiltration in experimental models of rodent intracerebral hemorrhage. *Exp Neurol* 2013; 241: 45–55.
22. Meguro T, Chen B, Lancon J, et al. Oxyhemoglobin induces caspase-mediated cell death in cerebral endothelial cells. *J Neurochem* 2001; 77: 1128–1135.
23. Cui Y, Duan X, Li H, et al. Hydrogen sulfide ameliorates early brain injury following subarachnoid hemorrhage in rats. *Mol Neurobiol* 2016; 53(6): 3646–3657.
24. Romero-Calvo I, Ocon B, Martinez-Moya P, et al. Reversible Ponceau staining as a loading control alternative to actin in Western blots. *Anal Biochem* 2010; 401: 318–320.
25. Harlow E and Lane D. Staining immunoblots for total protein using ponceau s. *CSH Protocols* 2006; 2006(1): pii: pdb.prot4269.
26. Shen H, Chen Z, Wang Y, et al. Role of neurexin-1beta and neuroligin-1 in cognitive dysfunction after subarachnoid hemorrhage in rats. *Stroke* 2015; 46: 2607–2615.
27. Yuan L, Le Bras A, Sacharidou A, et al. ETS-related gene (ERG) controls endothelial cell permeability via transcriptional regulation of the claudin 5 (CLDN5) gene. *J Biol Chem* 2012; 287: 6582–6591.
28. Mahajan SD, Tutino VM, Redae Y, et al. C5a induces caspase-dependent apoptosis in brain vascular endothelial cells in experimental lupus. *Immunology* 2016.
29. Solito E, Christian HC, Festa M, et al. Post-translational modification plays an essential role in the translocation of annexin A1 from the cytoplasm to the cell surface. *FASEB J* 2006; 20: 1498–1500.
30. Park JJ, Lim KH and Baek KH. Annexin-1 regulated by HAUSP is essential for UV-induced damage response. *Cell Death Dis* 2015; 6: e1654.
31. Caron D, Maaroufi H, Michaud S, et al. Annexin A1 is regulated by domains cross-talk through post-translational phosphorylation and SUMOYlation. *Cell Signall* 2013; 25: 1962–1969.
32. Deretic V, Jiang S and Dupont N. Autophagy intersections with conventional and unconventional secretion in tissue development, remodeling and inflammation. *Trends Cell Biol* 2012; 22: 397–406.
33. Li R, Tan S, Yu M, et al. Annexin A2 regulates autophagy in Pseudomonas aeruginosa infection through the Akt1-mTOR-ULK1/2 signaling pathway. *J Immunol* 2015; 195: 3901–3911.
34. Ghislat G, Aguado C and Knecht E. Annexin A5 stimulates autophagy and inhibits endocytosis. *J Cell Sci* 2012; 125: 92–107.
35. Li H, Huang S, Wang S, et al. Relationship between annexin A7 and integrin beta4 in autophagy. *Int J Biochem Cell Biol* 2013; 45: 2605–2611.
36. Schlunk F and Greenberg SM. The pathophysiology of intracerebral hemorrhage formation and expansion. *Transl Stroke Res* 2015; 6: 257–263.
37. Chen S, Yang Q, Chen G, et al. An update on inflammation in the acute phase of intracerebral hemorrhage. *Transl Stroke Res* 2015; 6: 4–8.
38. Xiong XY and Yang QW. Rethinking the roles of inflammation in the intracerebral hemorrhage. *Transl Stroke Res* 2015; 6: 339–341.
39. Shah K and Abbruscato T. The role of blood-brain barrier transporters in pathophysiology and pharmacotherapy of stroke. *Curr Pharm Des* 2014; 20: 1510–1522.
40. Cohen Z, Bonvento G, Lacombe P, et al. Serotonin in the regulation of brain microcirculation. *Progr Neurobiol* 1996; 50: 335–362.
41. Leak RK, Zheng P, Ji X, et al. From apoplexy to stroke: historical perspectives and new research frontiers. *Progr Neurobiol* 2014; 115: 1–5.

42. Hawkins BT and Davis TP. The blood-brain barrier/neurovascular unit in health and disease. *Pharmacol Rev* 2005; 57: 173–185.
43. Dorovkov MV and Ryazanov AG. Phosphorylation of annexin I by TRPM7 channel-kinase. *J Biol Chem* 2004; 279: 50643–50646.
44. Lu QY, Jin Y, Mao JT, et al. Green tea inhibits cycolooxygenase-2 in non-small cell lung cancer cells through the induction of Annexin-1. *Biochem Biophys Res Commun* 2012; 427: 725–730.
45. Zhao H, Garton T, Keep RF, et al. Microglia/macrophage polarization after experimental intracerebral hemorrhage. *Transl Stroke Res* 2015; 6: 407–409.
46. Pradel LA and Rendon A. Annexin 1 is present in different molecular forms in rat cerebral cortex. *FEBS Lett* 1993; 327: 41–44.
47. Zhang Z, Huang L, Zhao W, et al. Annexin 1 induced by anti-inflammatory drugs binds to NF-kappaB and inhibits its activation: anticancer effects in vitro and in vivo. *Cancer Res* 2010; 70: 2379–2388.
48. Pan B, Kong J, Jin J, et al. A novel anti-inflammatory mechanism of high density lipoprotein through up-regulating annexin A1 in vascular endothelial cells. *Biochim Biophys Acta* 2016; 1861: 501–512.